CHARMM Force Field Parameterization of Rosiglitazone

ANDERS HANSSON, PAULO C. T. SOUZA, RODRIGO L. SILVEIRA, LEANDRO MARTÍNEZ, MUNIR S. SKAF

Institute of Chemistry, State University of Campinas—UNICAMP, C.P. 6154, Campinas, SP 13084-862, Brazil

ABSTRACT: We develop a CHARMM-based interaction potential for rosiglitazone, a well-known selective ligand to the γ isoform of the peroxisome proliferator-activated receptor (PPARγ) and widely marketed antidiabetic drug of the thiazolidinedione (TZD) class. We derive partial atomic charges and dihedral torsion potentials for seven rotations in the molecule, for which there are no analogs available in CHARMM. The potential model is validated by performing a series of molecular dynamics simulations of rosiglitazone in neat water and of a fully solvated rosiglitazone-PPARγ complex. The structural and dynamical behavior of the complex is analyzed in comparison with available experimental data. The potential parameters derived here are readily transferable to a variety of pharmaceutically important TZD compounds. © 2010 Wiley Periodicals, Inc. Int J Quantum Chem 111: 1346–1354, 2011

Key words: rosiglitazone; TZD; CHARMM parameterization; nuclear receptors; PPARγ; molecular dynamics

1. Introduction

The nuclear receptor superfamily comprises a group of roughly 48 proteins responsible for regulation of gene transcriptional activity by means of hormone binding [1]. The γ isoform of the peroxisome proliferator-activated receptor (PPARγ) is a key receptor in the regulation of cell differentiation and proliferation [2]. PPARγ is also involved in inflammatory and immune responses and is highly expressed in various types of cancer and associated with type II diabetes [3]. PPARγ forms heterodimers with the retinoid X receptor (RXR), which is the necessary partner for DNA binding and transcription. RXR, activated by its natural ligand 9-*cis* retinoic acid, serves as heterodimeric partner for many nuclear receptors [1]. The more promiscuous PPARγ accommodates various types of ligands, mostly agonists.

Experimental techniques to identify novel ligands and to determine the crystal structure of

Correspondence to: M. S. Skaf; e-mail: skaf@iqm.unicamp.br
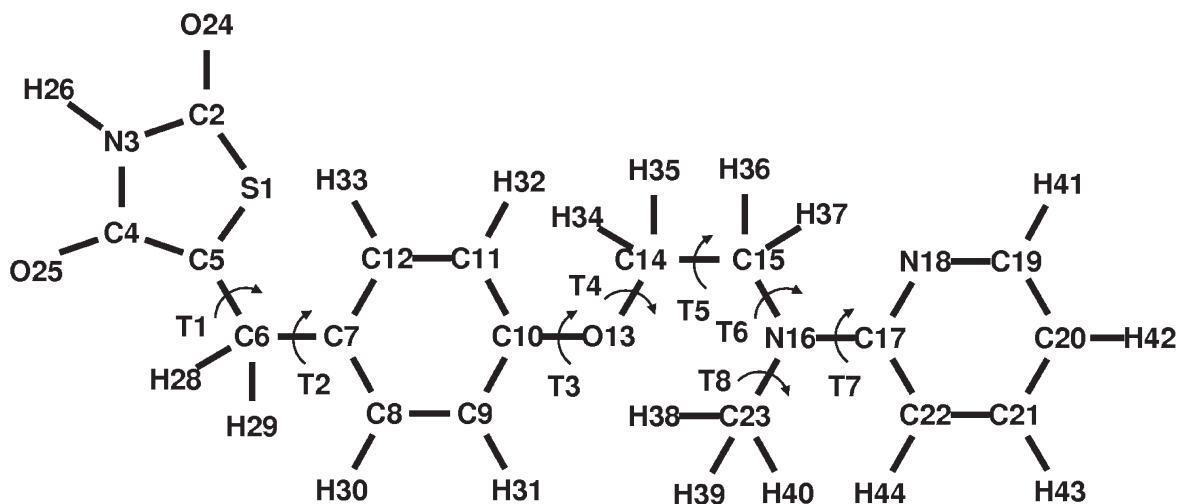
FIGURE 1. Chemical structure of rosiglitazone. The arc-shaped arrows indicate the torsion (T) of the eight bonds for which full revolution is possible.

receptors are quite advanced. However, the dynamic interactions of receptor, DNA response elements, and ligands remain poorly understood. Computational methods, such as molecular dynamics (MD), admit studies of association and dissociation processes [4–10], as well as the molecular mechanisms involved in receptor activation which give insight in ligand selectivity [11, 12]. The force fields primarily derived for molecular mechanics of macromolecules, such proteins, saccharides, lipids, and nucleic acids, do not provide parameters for specific chemical compounds, such as the thiazolidinediones (TZD), a well-known group of PPARγ agonists, of which rosiglitazone among others have been clinically studied and produced by the pharmaceutical industry [13].

The TZDs appear in two enantiomeric forms (R)-(+) and (S)-(−), due to the stereogenic center at atom C5 of the thiazolidine ring (Fig. 1). Higher antidiabetic activity have been predicted for the (S)-(−) enantiomer of rosiglitazone [14], which also is the observed form in the available crystallized PPARγ structures in the Protein Data Bank (PDB) [15]. Therefore, a complete set of parameters for the two enantiomers of rosiglitazone are derived here for future studies, especially the interactions the (S)-(−) enantiomer with nuclear receptors. The particular parameterization chosen for these simulations is based on the CHARMM force field for biomolecular systems [16]. The potential energy function is expressed by Eq. (1) as follows:

$$
V = \sum_{bonds} K_b(r - r_{0,b})^2 + \sum_{UB} K_{UB}(S - S_{0,UB})^2
$$
$$
+ \sum_{angle} K_a(\theta - \theta_{0,a})^2 + \sum_{dihedrals} K_{d,n}\left(1 + \cos\left(n\chi - \delta_{d,n}\right)\right)
$$
$$
+ \sum_{impropers} K_i\left(\psi - \psi_{0,i}\right)^2
$$
$$
+ \sum_{nonbonded} \varepsilon_{ij}\left[\left(\frac{R_{min,ij}}{r_{ij}}\right)^{12} - 2\left(\frac{R_{min,ij}}{r_{ij}}\right)^6\right] + \frac{q_iq_j}{4\pi\varepsilon_0 r_{ij}},
$$

$$(1)$$

where the sums extend to all bond stretchings, Urey-Bradley terms, angle bendings, dihedral torsions, improper dihedrals, and nonbonded van der Waals and Coulombic interactions. There are potential parameters developed for a great variety of biomolecules [17–20]. The transferability of parameters between molecules is the basic principle of these force fields, so parameters from similar molecules should be used whenever possible. However, for markedly flexible molecules, the sampling over different conformational states dependent critically on torsion (dihedral angle) potentials, so obtaining accurate torsional parameters derived from quantum mechanical potential energy surface (PES) scans of a given particular molecule is highly desirable [21].

In this work, we propose a complete set of CHARMM compatible force field parameters for rosiglitazone. Our main goal is to generate a force field for this molecule which is suitable for further computer simulation studies of the

interactions between the drug and its known target receptor and other proteins. Partial point charges are computed, CHARMM force field atom types assigned, and similar bond lengths, bond angles, Urey-Bradley, dihedral, and improper dihedral parameters for atom combinations not included in CHARMM are adopted. Finally, novel torsional parameters for seven dihedral rotations are derived based on CHARMM procedures. The newly parameterized model for rosiglitazone is tested by performing molecular dynamics (MD) simulations of this molecule in aqueous solutions and bound to the ligand binding domain (LBD) of PPARγ. We examine the simulated structure and dynamics of the rosigltazone-LBD complex in comparison with available experimental data and find that the proposed model is very-well behaved as far as these properties are concerned.

Because all TZDs share the same molecular backbone, the torsion potentials derived here are readily transferred to a series of pharmaceutically important compounds used in the treatment of type II diabetes, such as pioglitazone, troglitazone, rivoglitazone, and ciglitazone, to name few. There are two specific features in the molecular structure of the TZDs for which adequate CHARMM parameters were so far unavailable. One of them is the five-member heterocyclic aromatic ring containing S1 and N3 atoms for which there are neither CHARMM partial charges nor parameters for the T1 torsion (Fig. 1). On the other end of the molecule, there is an unusual pyridine ring containing a sp2 nitrogen (N18), also not available in CHARMM, which greatly affects the potential barrier for the T7 torsion (Fig. 1).

2. Parameterization and Computational Details

The force field parameters are developed at the restricted Hartree-Fock (RHF) ab initio level of theory with the 6-31G(d) basis set in consistency with the CHARMM parameterization of the c35b2 release. All ab initio calculations are performed with the Gaussian03 package revision E.01 [22], whereas classical force field potential energies are computed with the NAMD package [23], which is also used for the evaluative MD simulations. The acid dissociation constant (pK_a) of rosiglitazone is estimated with ALOGPS [24, 25].

For the self-consistent field (SCF) procedure, the default combination of the EDIIS and the CDIIS algorithms, with no damping or Fermi broadening, is used. The convergence criteria (in atomic units) are 1.0×10^{-6} for the energy, 1.0×10^{-6} for the maximum of density matrix, and 1.0×10^{-8} for the root mean square (RMS) of density matrix. The geometry is relaxed with the implemented version of the Berny geometry optimization algorithm and the convergence criteria (in atomic units) are 1.5×10^{-5} for maximum force, 1.0×10^{-5} for RMS force, 6.0×10^{-5} for maximum displacement, and 4.0×10^{-5} for RMS displacement. All four criteria were simultaneously satisfied.

Stationary points for RHF/6-31G(d) as well as with the more accurate 6-311G(d,p) basis set using both RHF and density functional theory DFT/B3LYP methods are obtained to evaluate the minimum of the first method. The partial point charge calculation is, however, based on the RHF/6-31G(d) geometry for consistency with CHARMM. Net atomic charges are derived to fit the RHF/6-31G(d) electrostatic potential of the relaxed structure. The sampling points are selected according to the employed Merz-Singh-Kollman approach [26, 27] in 10 layers and 17 grid point per unit area resulting in 95,155 points (the default is four layers and one point per unit area, giving 1,850 points for rosiglitazone.) The charges are also constrained to reproduce the molecular dipole moment. The atoms are classified in atom types of the CHARMM22 all-atom force field for proteins [17, 18] (release c35b2), based on the derived charges and the local chemical environment. Unavailable parameters are adopted primarily from similar groups of the all-atom force field for proteins CHARMM22 (release c35b2) and to less extent from CHARMM27 for nucleic acids [19, 20] and CHARMM32 for esters [28, 29] (of the same release).

The flexibility of the ligand is an important factor for their binding modes in the active site of the LBD and influence the ligand dissociation mechanism [4–7, 10]. The structure of rosiglitazone admits full revolution around eight bonds, as depicted in Fig. 1. The dihedral angle parameters required for describing the torsional barriers are not included in the current releases of CHARMM. Therefore, all torsional rotations, excluding the rotation of the CH_3 group, are parameterized. To avoid interference with the existing

dihedral parameters and to obtain unique set of dihedral angle parameters for the seven rotating bonds, a few atom type aliases are introduced.

To calculate the rotational energy profiles, the quadruples C4-C5-C6-C7, C5-C6-C7-C8, C9-C10-O13-C14, C10-O13-C14-C15, O13-C14-C15-N16, C14-C15-N16-C17, and C15-N16-C17-N18 define the dihedral torsions T1–T7, respectively. The energy profiles are obtained from rotational scans at 20 degree steps with a RHF/6-31G(d) geometry relaxation where only the regarded rotational angle is fixed. These energy profiles correspond to the total quantum mechanical potential energy, which in some cases differ substantially from the dihedral torsion potential energy, despite the relaxed geometry, mainly due to the constant point charge model. The missing classical dihedral torsion potential as follows:

$$V_d(\chi) = \sum_{n=1} K_{d,n}(1 + \cos(n\chi - \delta_{d,n})), \qquad (2)$$

is obtained for each dihedral torsion by least-square fitting this expression to the difference between the quantum and the molecular mechanics energy profiles. Since dihedral angle parameters are unknown for seven rotational barriers, the fitting procedure was conveniently done repeatedly, in a self-consistent manner, until convergence of all torsion potentials. The potential energy of the molecular mechanics force field is calculated with the NAMD2.7 package [23] via the NAMDENERGY plug-in of VMD [30]. Only terms with multiplicity $n \leq 6$ are considered and, as far as possible, phase angles δ are multiples of 180°, consistent with CHARMM. The obtained parameters for the dihedral angles defined by the aforementioned quadruples describe solely the total dihedral angle potential for each bond rotation. Hence, the other force constants of the involved dihedral angles are kept as zero.

Finally, MD simulations are performed to evaluate the developed parameters. Both rosiglitazone solvated in a box containing 1,828 water molecules at ambient conditions and rosiglitazone bound to the LBD of PPARγ (fully hydrated) are studied. The structure of the ligand–receptor complex, based on the ligand binding domain of the PDB structure 1FM6, chain D [31], is fully solvated by 18,000 water molecules, 28 Na$^+$ and 23 Cl$^-$ ions, reaching a concentration of ~0.15 mol/L to obtain a neutral system. Structural (crystallographic) water molecules within a distance of 4 Å from the protein are retained. The hydration shell around the protein is at least 15 Å thick and the entire system is enclosed in orthorhombic box with periodic boundary conditions. Langevin dynamics is employed to simulate the isothermal-isobaric ensemble at 300 K and 1.0 atm. The velocity Verlet algorithm is used for time integration with a time step of 2.0 fs. Full Coulomb forces are computed with the particle mesh Ewald algorithm [32], whereas van der Waals forces are truncated with a 12 Å smooth switching cutoff. The systems are initially relaxed with the default conjugate gradient and line search algorithm (CG) of NAMD2.7. We used the TIP3P model [33] for water and CHARMM parameters for the protein and counterions.

The following protocols are used for equilibrating the two systems. Rosiglitazone in water: (1) 300 steps of CG, keeping all atoms of rosiglitazone fixed; (2) 600 steps of CG, without any restraint; (3) 1,000 ps of MD without any restraint. The ligand–receptor complex in solvent: (1) 2,000 steps of CG, with all atoms of the protein fixed; (2) 200 ps of MD with all atoms of the protein fixed; (3) 500 steps of CG, with the Cα atoms fixed; (4) 200 ps of MD with the Cα fixed; (5) 400 ps of MD without any restraint. Finally, 6 ns MD simulations were performed starting from the equilibrated structures. The trajectories of first 1 ns of these simulations were discarded. This protocol was repeated 20 times for the ligand–receptor complex; thus, 20 independent 5 ns MD simulations were obtained for data analysis.

3. Results and Discussion

First the neutral state of (S)-(−)-rosiglitazone in neat water is considered. The structure is relaxed (in atomic units) to a maximum force of 1.0×10^{-6}, RMS force of 1.0×10^{-7}, maximum displacement of 1.9×10^{-5}, and RMS displacement of 0.3×10^{-5}. This geometry has total energy of −1478.1721 atomic units, which has converged to 0.37×10^{-8}, and its dipole moment is 3.014 D. On the basis of this configuration, we estimated the acid dissociation constants for rosiglitazone to 6.9 (base part) and 6.5 (acid part), as described above. The values are consistent with the literature [34]. At physiological pH around 7.4 [35], the unprotonated, neutral form of rosiglitazone (singlet state) predominates. Therefore, parameters

TABLE I

Atom names, CHARMM atom types, and partial atomic charges derived in this work.

Atom name	CHARMM type[a]	Charge (a.u.)	Atom name	CHARMM type[a]	Charge (a.u.)
S1	S	−0.21	C23	CT3	−0.17[b]
C2	C	0.60	O24	O	−0.48
N3	NH1	−0.62	O25	O	−0.55
C4	C	0.65	H26	H	0.40
C5	CT2	0.08	H27	HA	0.06
C6	CT2	−0.04	H28	HA	0.05
C7	CA	−0.13	H29	HA	0.06
C8	CA	0.01	H30	HP	0.12
C9	CA	−0.44	H31	HP	0.19
C10	CA	0.48	H32	HP	0.16
C11	CA	−0.37	H33	HP	0.11
C12	CA	−0.01	H34	HA	0.01
O13	OH1	−0.38	H35	HA	0.06
C14	CT2	0.21	H36	HA	0.12
C15	CT2	−0.14	H37	HA	0.08
N16	NC2	−0.35	H38	HA	0.12[c]
C17	C	0.91	H39	HA	0.09[c]
N18	NC2	−0.71	H40	HA	0.07[c]
C19	C	0.36	H41	HP	0.07
C20	CA	−0.55	H42	HP	0.20
C21	CA	0.23	H43	HP	0.11
C22	CA	−0.69	H44	HP	0.23

[a] CHARMM22 all-atom force field for proteins.
[b] −0.16 is used for the force field.
[c] 0.09 is used for the force field.

are derived for neutral rosiglitazone. Table I lists the calculated Merz-Singh-Kollman partial atomic charges for the ground state geometry. Despite the differentiated hydrogen charges of the CH_3 groups, the average 0.09 is adopted for all methyl hydrogens, yielding −0.16 for the methyl carbons. The ground state geometry at RHF and B3LYP level using the 6-311G(d,p) basis set confirm above calculated molecular conformation.

The atoms are classified in atom types of the CHARMM22 all-atom force field for proteins (release c35b2) based on the derived charges and the local chemical environment (Table I). Bond, angle, and dihedral parameters (excluding T1–T7 dihedral angles discussed below), as well as Urey-Bradley distances and Lennard-Jones energy and distance parameters, which could be obtained by group analogy from the CHARMM force field, are provided as Supporting Information.

The calculated dihedral angle PES for the torsions T1–T7 and the corresponding fitting functions [Eq. (2)] are depicted in Fig. 2. The top panel (T3) also shows the ab initio quantum mechanical PES (black dots), the molecular mechanics PES excluding the dihedral potential for the T3 torsion (crosses), the quantum and classical PES difference (plus signs) and the adjusted dihedral potential (solid line). For comparison, the full molecular mechanics PES, now including the parameterized torsional potential, is shown by empty circles. The agreement between the quantum and the full classical force filed PESs is excellent. In the remainder panels, only the quantum and classical PESs differences (plus signs) and the adjusted potentials (lines) are shown. As mentioned in "Parameterization and Computational Details," we have applied the CHARMM restriction of using the first six terms in the fitting function [cf., Eq. (2)], which limits quality of the fit. Moreover, the adjustments of the torsion parameters have been carried out in a self-consistent way due to the mutual dependence between the distinct rotations. The complete set of fitted parameters thus obtained is listed in Table II.

The first test for the force field is performed by examining the behavior of rosiglitazone in an
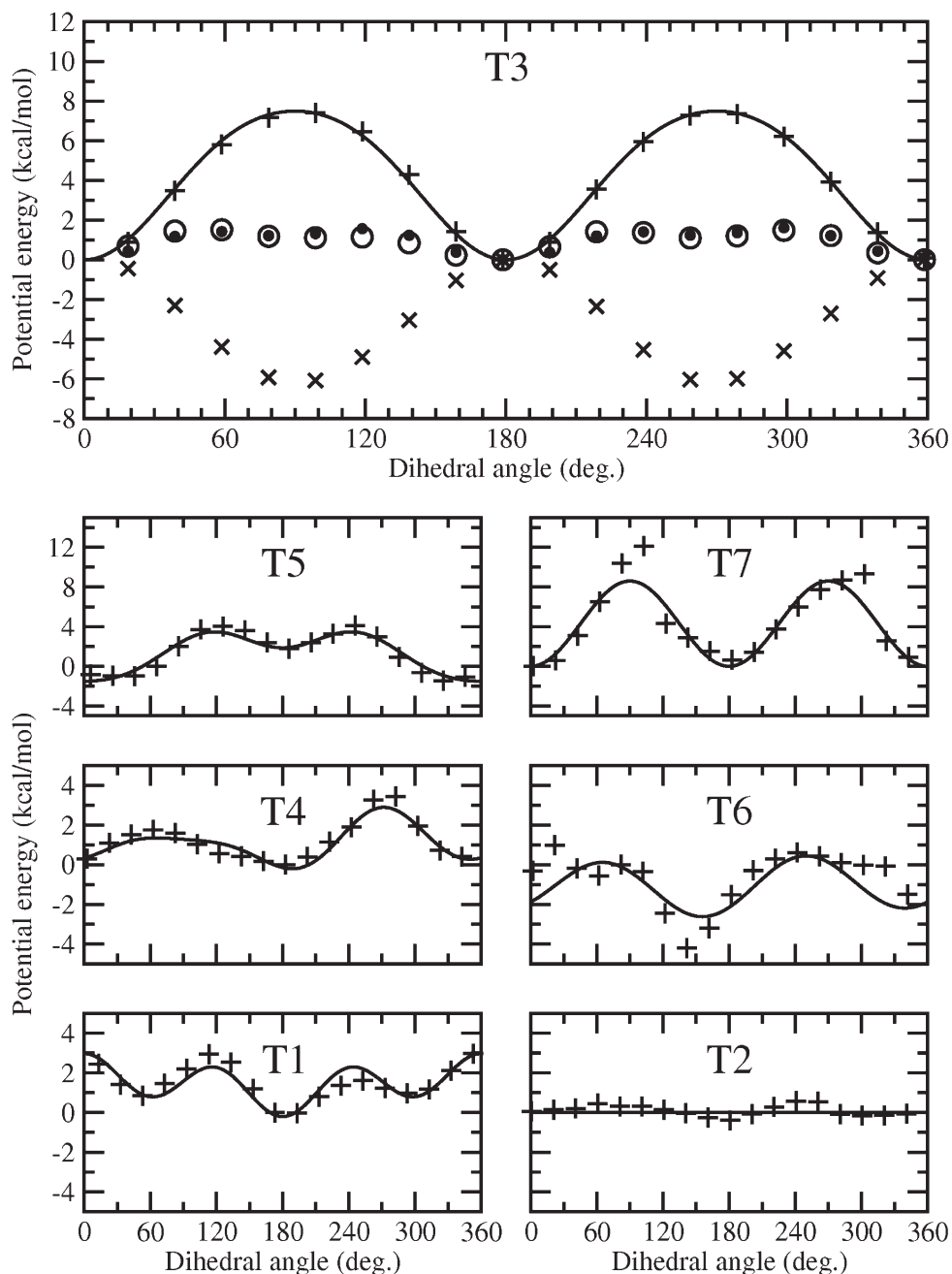
FIGURE 2. Torsion energies of the bonds C5-C6 (T1), C6-C7 (T2), C10-O13 (T3), O13-C14 (T4), C14-C15 (T5), C15-N16 (T6), and N16-C17 (T7). The black dots represent the ab initio PES, whereas the crosses (x) indicate the force field PES without the considered dihedral angle. The difference between them is shown by plus signs (+) and the adjusted potential energy of the dihedral angle is depicted by a solid line. For comparison, the circles show the total force field, including the parameterized dihedral angle.

aqueous environment. The average geometry of the molecule in water closely replicates the ab initio relaxed geometry after the initial relaxation of the system. Structural aligning of the geometries, where all atoms are taken into account,
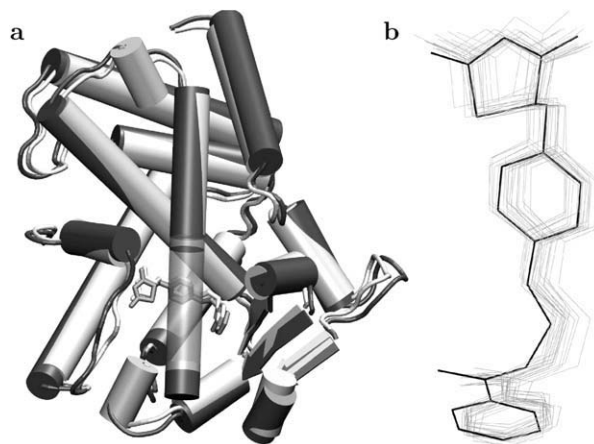
gives a root mean square deviation (RMSD) of only 0.18 Å. The planarity of the three rings is maintained during the simulation, so no additional improper dihedral angles are therefore included.

TABLE II
**Dihedral parameters for seven torsional rotations.**

Dihedral angle	$K_{d,n}$ (kcal/mol)	N	δ (°)
T1: C4 C5 C6 C7	0.5659	1	0.0
	−0.0987	2	0.0
	1.0226	3	0.0
T2: C5 C6 C7 C8	0.0000	1	0.0
T3: C9 C10 O13 C14	3.7459	2	180.0
	0.3416	4	180.0
T4: C10 O13 C14 C15	0.4826	1	−60.0
	0.9938	2	180.0
	−0.3873	3	−90.0
T5: O13 C14 C15 N16	2.1289	1	180.0
	−1.1948	2	0.0
	0.8041	3	0.0
	−0.3619	4	180.0
T6: C14 C15 N16 C17	0.2725	1	−60.0
	−1.3384	2	−45.0
T7: C15 N16 C17 N18	4.2932	2	180.0

FIGURE 3. (a) Average structure of the PPARγ-rosiglitazone complex from simulations (light gray) superimposed to the crystallographic structure (dark gray). (b) Average structures of rosiglitazone for individual 5 ns simulations (light gray) and the crystal structure (black), with the LBDs structurally aligned.

The main evaluation comes from examining the behavior of the ligand and its target nuclear receptor protein PPARγ in the ligand–receptor complex. In all currently reported structures in PDB containing rosiglitazone (PDB IDs: 1FM6, 1ZGY, 2PRG, 3CS8, and 3DZY), it appears bounded to the LBD pocket of PPARγ. One of the highest resolution structures of the ligand-LBD complex is the 1FM6 structure, with a resolution of 2.10 Å. Therefore, our evaluative simulations of rosiglitazone interacting with the PPARγ LBD start from the 1FM6 structure.

The average structure of the rosiglitazone-LBD complex over 20 independent 5 ns simulations yields a RMSD of only 0.99 Å after a structural alignment with the initial crystal structure [Fig. 3(a)]. The RMSD between the average simulated and crystal structures of rosiglitazone itself is only ~0.35 Å. The average structure of rosiglitazone obtained from each 5 ns simulation and the crystal structure are visualized in Fig. 3(b), after alignment of the LBDs, indicating that the PPARγ LBD remains very stable and structurally well-correlated with the crystallographic structure in the presence of the parameterized ligand. In addition, the average conformation and position of rosiglitazone inside the ligand binding pocket (i.e., the ligand binding mode), preserve the crystal conformation and the crystalline ligand-LBD contacts. These results indicate that the ligand–protein and ligand intramolecular interactions are well accounted for by the proposed interaction potential.

The available experimental data of rosiglitazone regarding its dynamical behavior is limited to the crystallographic Debye-Waller or temperature B-factors. A comparison between the crystallographic and simulated B-factors is presented in Fig. 4, showing very good agreement, apart from an overall multiplicative factor, which is common in this type of comparison because the crystallographic B-factors depend on the structure resolution. The mobility of the different structural elements of the LBD derived from diffraction data are well-reproduced by the motions of rosiglitazone obtained from the MD simulations with the proposed model.
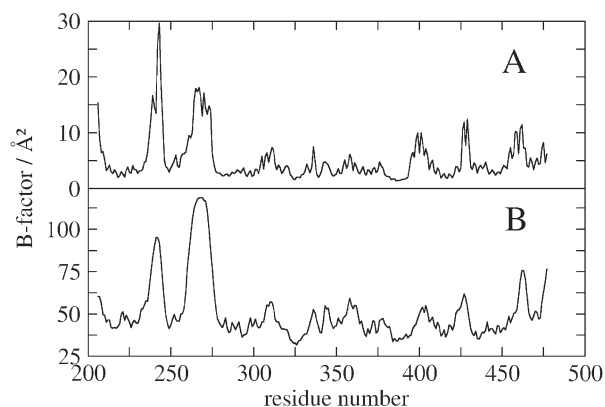
FIGURE 4. Temperature B-factors obtained from the present simulations (A) and available from crystallography experiments (PDB ID: 1FM6) (B).

4. Conclusions

A CHARMM-based model has been derived for molecular simulations of rosiglitazone, an important nuclear receptor ligand, with relevant pharmaceutical applications in the treatment of type II diabetes. The proposed force field enables MD studies of the interactions of rosiglitazone and other TZD compounds with the nuclear receptor PPARγ, as well as with other proteins and other biomolecular systems under CHARMM. We have specially focused on the energy profiles of the rotating bonds, which give the molecule its characteristic flexibility and are very significant factors for ligand association/dissociation mechanisms and other features that depend on ligand conformational adaptations. MD simulations are being carried out for the rosiglitazone-PPARγ complex using this potential aiming to investigate the concerted motions of different structural elements of the LBD intermediated by rosiglitazone in the binding pocket and the pathways of ligand dissociation from the PPARγ LBD core.

References

1. Ribeiro, R. C. J.; Kushner, P. J.; Baxter, J. D. Annu Rev Med 1995, 46, 443.

2. Roberts-Thompson, S. J. Immunol Cell Biol 2000, 78, 436.

3. Parker, J. C. Adv Drug Deliv Rev 2002, 54, 1173.

4. Blondel, A.; Renaud, J. P.; Fischer, S.; Moras, D.; Karplus, M. J Mol Biol 1999, 291, 101.

5. Kosztin, D.; Israilev, K. S.; Schulten, K. Biophys J 1999, 76, 188.

6. Martínez, L.; Sonoda, M. T.; Webb, P.; Skaf, M. S.; Polikarpov, I. Biophys J 2005, 89, 2011.

7. Martínez, L.; Webb, P.; Polikarpov, I.; Skaf, M. S. J Med Chem 2006, 49, 23.

8. Sonoda, M. T.; Martínez, L.; Webb, P.; Skaf, M. S.; Polikarpov, I. Mol Endocrinol 2008, 22, 1565.

9. Carlsson, P.; Burendahl, S.; Nilsson, L. Biophys J 2006, 9, 3151.

10. Martínez, L.; Polikarpov, I.; Skaf, M. S. J Phys Chem B 2008, 112, 10741.

11. Bleicher, L.; Aparicio, R.; Nunes, F. M.; Martínez, L.; Dias, S. M. G.; Figueira, A. C. M.; Santos, M. A. M.; Venturelli, W. H.; Silva, R.; Donate, P. M.; Neves, F. A. R.; Simeoni, L. A.; Baxter, J. D.; Webb, P.; Skaf, M. S.; Polikarpov, I. BMC Struct Biol 2008, 8, 8.

12. Martínez, L.; Nascimento, A. S.; Nunes, F. M.; Phillips, K.; Aparicio, R.; Dias, S. M. G.; Figueira, A. C. M.; Lin, J. H.; Nguyen, P.; Apriletti, J. W.; Neves, F. A. R.; Baxter, J. D.;

13. Webb, P.; Skaf, M. S.; Polikarpov, I. Proc Natl Acad Sci USA 2009, 106, 20717.

13. Houseknetch, K. L.; Cole, B. M.; Steele, P. J. Domest Anim Endocrinol 2002, 22, 1.

14. Parks, D. J.; Tomkinson, N. C. O.; Villeneuve, M. S.; Blanchard, S. G.; Willson, T. M. Bioorg Med Chem Lett 1998, 8, 3657.

15. The Protein Data Bank (PDB) archive, [online] Available at: http://www.pdb.org.

16. Brooks, B. R.; Brooks, C. L., III; Mackerell, A. D., Jr.; Nilsson, L.; Petrella, R. J.; Roux, B.; Won, Y.; Archontis, G.; Bartels, C.; Boresch, S.; Caflisch, A.; Caves, L.; Cui, Q.; Dinner, A. R.; Feig, M.; Fischer, S.; Gao, J.; Hodoscek, M.; Im, W.; Kuczera, K.; Lazaridis, T.; Ma, J.; Ovchinnikov, V.; Paci, E.; Pastor, R. W.; Post, C. B.; Pu, J. Z.; Schaefer, M.; Tidor, B.; Venable, R. M.; Woodcock, H. L.; Wu, X.; Yang, W.; York, D. M.; Karplus, M. J Comput Chem 2009, 30, 1545.

17. MacKerell, A. D., Jr.; Feig, M.; Brooks, C. L. J Comput Chem 2004, 25, 1400.

18. MacKerell, A. D., Jr.; Bashford, D.; Bellott, M.; Dunbrack, R. L., Jr.; Evanseck, J. D.; Field, M. J.; Fischer, S.; Gao, J.; Guo, H.; Ha, S.; Joseph-McCarthy, D.; Kuchnir, L.; Kuczera, K.; Lau, F. T. K.; Mattos, C.; Michnick, S.; Ngo, T.; Nguyen, T. D.; Prodhom, B.; Reiher, W. E., III; Roux, B.; Schlenkrich, M.; Smith, J. C.; Stote, R.; Straub, J.; Watanabe, M.; Wiórkiewicz-Kuczera, J.; Yin, D.; Karplus, M. J Phys Chem B 1998, 102, 3586.

19. Foloppe, N.; MacKerell, A. D., Jr. J Comput Chem 2000, 21, 86.

20. MacKerell, A. D., Jr.; Banavali, N. K. J Comput Chem 2000, 21, 105.

21. Guvench, O.; MacKerell, A. D., Jr. J Mol Model 2008, 14, 667.

22. Frisch, M. J.; Trucks, G. W.; Schlegel, H. B.; Scuseria, G. E.; Robb, M. A.; Cheeseman, J. R.; Montgomery, J. A., Jr.; Vreven, T.; Kudin, K. N.; Burant, J. C.; Millam, J. M.; Iyengar, S. S.; Tomasi, J.; Barone, V.; Mennucci, B.; Cossi, M.; Scalmani, G.; Rega, N.; Petersson, G. A.; Nakatsuji, H.; Hada, M.; Ehara, M.; Toyota, K.; Fukuda, R.; Hasegawa, J.; Ishida, M.; Nakajima, T.; Honda, Y.; Kitao, O.; Nakai, H.; Klene, M.; Li, X.; Knox, J. E.; Hratchian, H. P.; Cross, J. B.; Bakken, V.; Adamo, C.; Jaramillo, J.; Gomperts, R.; Stratmann, R. E.; Yazyev, O.; Austin, A. J.; Cammi, R.; Pomelli, C.; Ochterski, J. W.; Ayala, P. Y.; Morokuma, K.; Voth, G. A.; Salvador, P.; Dannenberg, J. J.; Zakrzewski, V. G.; Dapprich, S.; Daniels, A. D.; Strain, M. C.; Farkas, O.; Malick, D. K.; Rabuck, A. D.; Raghavachari, K.; Foresman, J. B.; Ortiz, J. V.; Cui, Q.; Baboul, A. G.; Clifford, S.; Cioslowski, J.; Stefanov, B. B.; Liu, G.; Liashenko, A.; Piskorz, P.; Komaromi, I.; Martin, R. L.; Fox, D. J.; Keith, T.; Al-Laham, M. A.; Peng, C. Y.; Nanayakkara, A.; Challacombe, M.; Gill, P. M. W.; Johnson, B.; Chen, W.; Wong, M. W.; Gonzalez, C.; Pople, J. A. Gaussian 03, Revision E. 01; Gaussian, Inc.: Wallingford, CT, 2004.

23. Phillips, J. C.; Braun, R.; Wang, W.; Gumbart, J.; Tajkhorshid, E.; Villa, E.; Chipot, C.; Skeel, R. D.; Kale, L.; Schulten, K. J Comput Chem 2005, 26, 1781.

24. Tetko, I. V.; Gasteiger, J.; Todeschini, R.; Mauri, A.; Livingstone, D.; Ertl, P.; Palyulin, V. A.; Radchenko, E. V.; Zefirov, N. S.; Makarenko, A. S.; Tanchuk, V. Y.; Prokopenko, V. V. J Comput Aided Mol Des 2005, 19, 453.

25. VCCLAB's online software Alogps 2.1 (2005), [online] Available at: http://www.vcclab.org.

26. Singh, U. C.; Kollman, P. A. J Comput Chem 1984, 5, 129.

27. Besler, B. H.; Merz, K. M., Jr.; Kollman, P. A. J Comput Chem 1990, 11, 431.

28. Vorobyov, I.; Anisimov, V. M.; Greene, S.; Venable, R. M.; Moser, A.; Pastor, R. W.; MacKerell, A. D., Jr. J Chem Theory Comput 2007, 3, 1120.

29. Lee, H.; Venable, R. M.; MacKerell, A. D., Jr.; Pastor, R. W. Biophys J 2008, 95, 1590.

30. Humphrey, W.; Dalke, A.; Schulten, K. J Mol Graph 1996, 14, 33.

31. Gampe, R. T., Jr.; Montana, V. G.; Lambert, M. H.; Miller, A. B.; Bledsoe, R. K.; Milburn, M. V.; Kliewer, S. A.; Willson, T. M.; Xu, H. E. Mol Cell 2000, 5, 545.

32. Darden, T.; York, D.; Pedersen, L. J. J Chem Phys 2003, 98, 10089.

33. Jorgensen, W. L.; Chandrasekhar, J.; Madura, J. D. J Chem Phys 1983, 79, 926.

34. Block, J. H.; Beale, J. M., Jr., Eds. Wilson and Gisvolds Textbook of Organic Medicinal and Pharmaceutical Chemistry, 11th ed.; Lippincott Williams & Wilkins: Philadelphia, 2004.

35. Voet, D.; Voet, J. G.; Pratt, C. Fundamentals of Biochemistry; Wiley: New York, 1999.